REPORT DOCUMENTATION PAGE

Form Approved
OMB No. 0704-0188

1. REPORT DATE *(DD-MM-YYYY)*	2. REPORT TYPE	3. DATES COVERED *(From - To)*
08-12-2008	Technical Paper & Briefing Charts	

4. TITLE AND SUBTITLE

Effect of Variable Phase Transverse Acoustic Fields on Coaxial Jet Forced Spread Angles (Preprint)

5a. CONTRACT NUMBER

5b. GRANT NUMBER

5c. PROGRAM ELEMENT NUMBER

6. AUTHOR(S)
Juan I. Rodriguez, Jeffrey Graham, Ivett A. Leyva, & Douglas Talley (AFRL/RZSA)

5d. PROJECT NUMBER

5f. WORK UNIT NUMBER
23080533

7. PERFORMING ORGANIZATION NAME(S) AND ADDRESS(ES)

Air Force Research Laboratory (AFMC)
AFRL/RZSA
10 E. Saturn Blvd.
Edwards AFB CA 93524-7680

8. PERFORMING ORGANIZATION REPORT NUMBER

AFRL-RZ-ED-TP-2008-579

9. SPONSORING / MONITORING AGENCY NAME(S) AND ADDRESS(ES)

Air Force Research Laboratory (AFMC)
AFRL/RZS
5 Pollux Drive
Edwards AFB CA 93524-7048

10. SPONSOR/MONITOR'S ACRONYM(S)

11. SPONSOR/MONITOR'S NUMBER(S)
AFRL-RZ-ED-TP-2008-579

12. DISTRIBUTION / AVAILABILITY STATEMENT

Approved for public release; distribution unlimited (PA #08475A).

13. SUPPLEMENTARY NOTES
For presentation at the 47th AIAA Aerospace Sciences Meeting and Exhibit, Orlando, FL, 5-8 January 2009.

14. ABSTRACT

An experimental study on the effects of a variable phase transverse acoustic field on the inner jet spreading angle of a N_2 shear coaxial jet at nearcritical pressures is presented. The jet spreading angle is an important parameter which characterizes the mixing between two flows. The transverse acoustic field is generated by two piezo-sirens which have a variable phase between them so the position of the jet with respect to the pressure and velocity field can be adjusted. The main parameter investigated is the spreading angle of the dark inner jet core. The angle measurements are made from approximately 1000 backlit images. The shear coaxial injector used here is similar to those used in cryogenic liquid rockets. The acoustic field is driven at a frequency of 3.0 ± 0.1 kHz. It was observed that acoustic forcing has the strongest effect on the inner jet spreading angles at moderate values of the outer to inner jet momentum flux ratio, providing further evidence of the existence of a regime where the inner jet is most vulnerable to acoustic excitation effects.

15. SUBJECT TERMS

16. SECURITY CLASSIFICATION OF:			17. LIMITATION OF ABSTRACT	18. NUMBER OF PAGES	19a. NAME OF RESPONSIBLE PERSON
a. REPORT	b. ABSTRACT	c. THIS PAGE			Dr. Douglas Talley
Unclassified	**Unclassified**	**Unclassified**	SAR	35	19b. TELEPHONE NUMBER *(include area code)* N/A

Effect of Variable Phase Transverse Acoustic Fields on Coaxial Jet Forced Spread Angles (Preprint)

Juan I Rodriguez[1], Jeffrey J Graham[2], Ivett A. Leyva[3] and Douglas Talley[4]
Air Force Research Laboratory, Edwards AFB, CA 93524

An experimental study on the effects of a variable phase transverse acoustic field on the inner jet spreading angle of a N_2 shear coaxial jet at nearcritical pressures is presented. The jet spreading angle is an important parameter which characterizes the mixing between two flows. The transverse acoustic field is generated by two piezo-sirens which have a variable phase between them so the position of the jet with respect to the pressure and velocity field can be adjusted. The main parameter investigated is the spreading angle of the dark inner jet core. The angle measurements are made from approximately 1000 backlit images. The shear coaxial injector used here is similar to those used in cryogenic liquid rockets. The acoustic field is driven at a frequency of 3.0 ± 0.1 kHz. It was observed that acoustic forcing has the strongest effect on the inner jet spreading angles at moderate values of the outer to inner jet momentum flux ratio, providing further evidence of the existence of a regime where the inner jet is most vulnerable to acoustic excitation effects.

I. Introduction

THE study of coaxial jet behavior is of fundamental importance for the understanding of liquid rocket engines (LRE's), since coaxial jet injectors are used in a variety of LRE's, including the Space Shuttle Main Engine. Essential parameters to consider when using a coaxial jet injector are the momentum flux ratio and the conditions of the combustion chamber. Knowing approximate values of these parameters is important in the early stages of LRE's design so that factors such as propellant mixing behavior and predisposition to combustion instabilities can be assessed. Improvement of LRE's performance has driven the mean combustion chamber pressure of these devices to conditions where propellants reach a supercritical state. Thus, the following study investigates the influence of parameters such as momentum flux ratio between the outer and inner jet and mean combustion chamber pressure in the spreading angles of coaxial jets.

Spreading angles have been studied previously by Chehroudi et al.[1] and others. Chehroudi's group presented an extensive study of single round jets spanning subcritical to supercritical pressures, including experimental data on variable-density gas-gas jets from different researchers in which the main variable investigated was the ratio of the chamber density to the jet density. This parameter is important when considering the interaction between a single jet and a quiescent atmosphere. It was shown that for jets at supercritical pressure and temperature the spreading angle growth rate agreed quantitatively with the predictions of the other research efforts before. In the case of a coaxial jet, the inner jet spreading angle is also an important parameter since it is an indication of the growth of the shear layer between the inner and outer streams. Gutmark et al.[2] concluded in their coaxial vs. free jet studies that in coaxial flow configurations more of the surrounding fluid is entrained deeper into the inner jet as compared to the free jet case, enhancing the overall mixing process. These researchers also found that the geometry of the injector plays a role as well, with better mixing performance achieved by rectangular injectors compared to circular ones. Gautam and Gupta[3] reported in their cryogenic coaxial injector studies at atmospheric pressures an increase in the evaporation of the inner jet and enhanced mixing with the surrounding flow with increasing outer to inner

[1] Graduate Student, UCLA/ AFRL, Edwards AFB, CA 93524, AIAA Student Member
[2] Combustion Research Scientist, AFRL/RZSA, Edwards AFB, CA 93524
[3] Lead, Combustion Group, AFRL/RZSA, Edwards AFB, CA 93524, AIAA Senior Member
[4] Sr. Aerospace Engineer, AFRL/RZSA, Edwards AFB, CA 93524, AIAA Member

momentum flux ratio (J). They also change the geometry of their injector setup by modifying the recess length between the inner jet and the outer jet exits. They found that larger recess lengths promote higher jet expansion and more entrainment of surrounding gases into the flow. Their shear layer analysis confirms that mixing and jet expansion are slower at lower J's. Zong and Yang[4] also find in their numerical study of high pressure coaxial reactive flow that as the J increases, turbulent mixing is enhanced whereas the inner jet dark core is reduced. Finally, Richecoeur et al.[5] studied an acoustically excited, multiple element, and reactive coaxial injector configuration at elevated but still subcritical pressure conditions. They found that conditions where combustion became sensitive to external oscillations happened at lower J's. The strong coupling between acoustics and combustion showed an enhancement of the flame spread which might be associated with improved mixing. However, for combustion instabilities these "enhanced" mixing might be something to avoid.

This paper focuses on the effects of both the magnitude and gradient of the pressure and velocity fields of an acoustically forced coaxial jet flow, specifically on the inner jet spreading angles at nearcritical pressures. An earlier study analyzed the behavior of the inner jet spreading angles at subcritical pressures[6]. In these studies, we vary the magnitude and relative position of the jet with respect to the pressure and velocity acoustic field by alternating the phase between the two acoustic resonators. It has been observed by Leyva et al.[7,8] that the effects of acoustics on the dark core length were the greatest at subcritical pressures and for certain range of momentum flux ratios ($1 < J < 4$). This study includes spreading angle results for near-critical and supercritical pressures in the $0.6 < J < 10$ range. Because of the added complexity introduced when working with mixtures, N_2 is used as the sole working fluid in this study.

II. Experimental Setup

The experimental studies reported in this paper were performed at the Air Force Research Laboratory (AFRL) located at Edwards Air Force Base, CA. The Cryogenic Supercritical Laboratory (EC-4) was the location where the test took place. An overview of the test section is shown in Fig. 1. Gaseous N_2 is used to supply the inner and outer jet flows and to pressurize the chamber. The outer and inner jets are cooled by two or three heat exchangers (HE's) depending on the plumbing configuration ran. The coolant for both the inner and outer jet is liquid nitrogen obtained from a cryogenic tank. One heat exchanger cools the inner jet and the other two cool the outer jet. The temperature (T) of the two jets is controlled by adjusting the flow rate of liquid nitrogen through the HE's. The mass flow rate through the inner and outer jets is measured, before they are cooled, with Porter mass flow meters (122 and 123-DKASVDAA), since it was found that it is much easier to measure the flow rates at ambient rather than at cryogenic temperatures. The chamber pressure is measured with a Stellar 1500 transducer. To keep the amplitude of the acoustic oscillations to a maximum near the jet, an inner chamber was created (Fig. 1). This inner chamber has a nominal height of 6.6cm, a width of 7.6cm and a depth of 1.3cm.

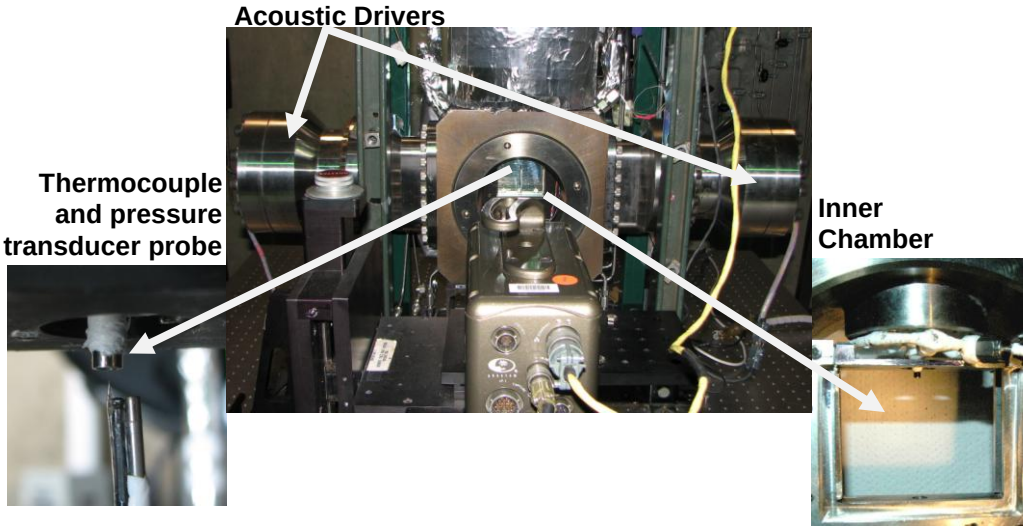

Figure 1. Overview of the Main Chamber of the Supercritical Flow Facility, EC-4 at AFRL/Edwards.

Details for the coaxial injector used are shown in Fig. 2. The inner diameter of the inner jet, D1, is 0.51 mm. The outer jet has an inner diameter, D2, of 1.59 mm and outer diameter, D3, of 2.42 mm. The length to inside diameter ratio is 100 for the inner jet and 67 for the outer jet (taking as reference the mean width of the annular passage). There is a small bias of about 8% of the mean gap width. The inner jet is recessed by 0.3 mm from the outer jet. The temperature of the jets is measured with an unshielded type E thermocouple which has a bead diameter of 0.1mm. It is measured from the bottom so the thermocouple tip can get as close to the exit plane as possible. Thus, the thermocouple can measure the temperature within the recess of the inner jet. The accuracy of this thermocouple was checked with an RTD and found to be ±1 K. The average distance from the exit plane, denoted H in Fig. 2 is ~ 0.3 mm. A Kulite XQC-062 pressure transducer is placed next to the thermocouple and used to measure the pressure at a sampling frequency of 20 kHz. Both the pressure transducer and the thermocouple are moved in the plane perpendicular to the jet axis with a piezo positioning system built by Attocube Systems which can move a total distance of 3mm in 1 dimension with step sizes in the order of 0.01mm. Properties such as density, viscosity, and surface tension are computed from the measured flow rates, chamber pressure and jet temperature, using NIST's REFPROP[9]. From this, the velocity ratio (VR) and J for a given condition can be computed.

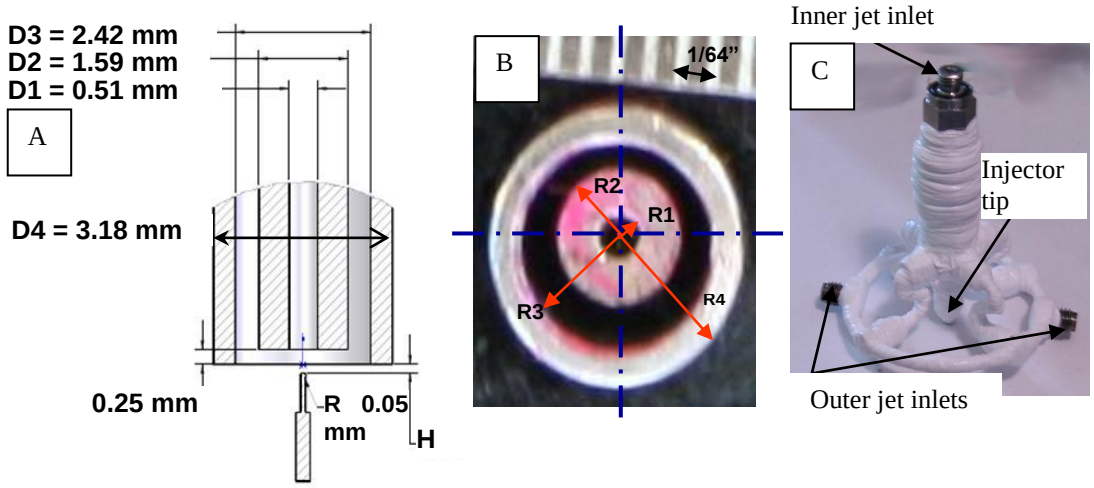

Figure 2. Coaxial injector used for the present study.

The jet is visualized by taking backlit images using a Phantom 7.1 CMOS camera. The resolution of the images varies from 128x224 to 196x400 depending on chamber pressure and J, which in turn determines the size of the visible features of the jet that this study is characterizing. Each pixel represents an area of about 0.08 mm x 0.08 mm with a framing rate of 20, 25 or 41 kHz. The jet is backlit using a Newport variable power arc lamp set at 160 or 300 W. The acoustic waves are generated using two piezo-sirens custom-designed for AFRL by Hersh Acoustical Engineering, Inc. (Fig.1). For these acoustic sources a piezo-ceramic element is externally excited with a sinusoidal wave at the desired driving frequency for the system. This frequency is chosen by manually varying the frequency on a signal generator until the highest amplitudes for the pressure waves are obtained. This signal is amplified and then fed to the piezo-siren. The movement of the piezo element is transmitted to the aluminum cone attached to it, and the cone then produces acoustics waves. To accommodate for the rectangular chamber a waveguide with a catenary contour is used to guide the waves from a circular cross-section to a rectangular cross-section (also shown in Fig.1). The sound acoustic pressure in the inner chamber ranges from 7 to 30 kilopascals (1 to 5 psi) peak-to-peak at ~ 3.0 kHz.

III. Discussion

The results presented in this paper were obtained by driving the coaxial jet transversely with two identical acoustic sources whose phase can be changed arbitrarily. Theoretically, when the two sources have a zero degree phase angle, then the movement of the cones themselves could be described as "towards each other" as presented in

Figure 3. At the other extreme, when the two sources are at 180 degrees out of phase, then the motion could be seen as "chasing" each other. For all cases, the two acoustic sources are fed with constant voltages throughout the phase changes.

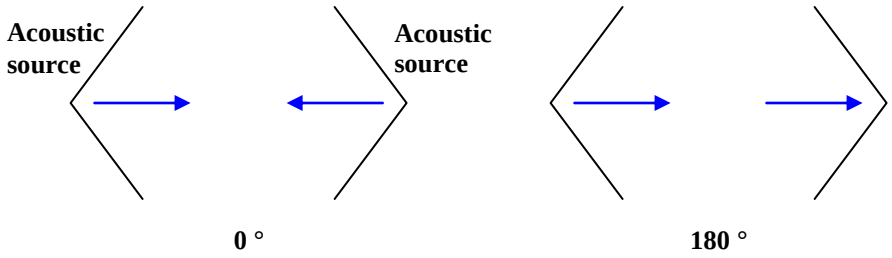

Figure 3. Schematic of the two acoustic sources with phase angles of 0° and 180° between them.

Dark Core Spreading Angle

To obtain the inner jet spread angles for a given condition, 998 images such as the one shown in Fig. 4a were used. A raw image is converted to a black and white image using an image processing technique previously described in detail in Leyva et al.[7,8]. From the black and white image, a contour of the dark core is constructed as shown in Fig. 4c. We use the dark core to describe the behavior of the inner jet since for our experiments the inner jet is always colder, thus denser, than the outer jet and appears darker in the backlit images. In order to measure the two angles, first, the locations of the left and right contours were recorded for each image as pictured in Fig. 4d. Then, for each row, the leftmost and rightmost contour points from all 998 images were selected to build a "maximum left contour" and a "maximum right contour" as can be seen in Fig. 5.

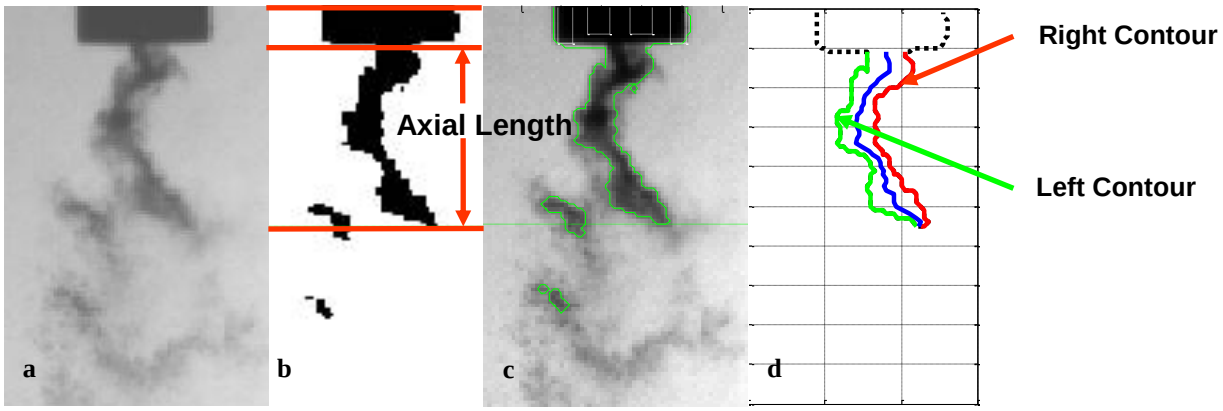

Figure 4a. Raw image from high-speed camera. 4b. Black and white conversion after image processing. 4c. Dark core boundary extracted from the processed black and white image. 4c. Schematic of the left and right contours used in this study.

A linear fit through each contour was used to calculate the left and right spread angles. In Fig. 5 the two angles measured, α_{Left} and α_{Right}, are shown. The linear fit was chosen to start where the contour was the thinnest. This usually took place between ½ D1 (in supercritical cases at high Js, for example) up to 5 D1 (for cases at moderate Js) and ended at the mean axial dark core length which is calculated by averaging the extracted axial length (see Fig. 4b) of all 998 images for each case. The axial dark core length is the axial projection of the dark core region connected to the injector and is also carefully explained in Leyva et al.[7,8]. An important reason for not choosing the first row of the contour to start the linear fit but begin a few inner jet diameters downstream was to minimize the effect of a recirculation zone that is generated due to the geometry of our injector. This recirculation occurs due to a thick inner jet post which prevents the inner jet and outer jet from coming into contact right away

after the inner jet post ends. The recirculation region appears just as dark as the inner jet dark core and biases the measurements. By starting the linear fit where the contour is the thinnest we expect to avoid some of that bias.

Once the limits for the linear fit are chosen, a line is obtained and the angle associated with it is obtained. Both left and right angles computed in this manner are shown in Fig. 5. It is the sum of both left and right angles what is referred to in this study as the "inner jet spreading angle". This computed spread angle represents the region the inner jet traveled during the amount of time it took to record the 998 images. For the case of no acoustics, we call it 'maximum baseline spread angle'. It is important to note that this 'maximum baseline spread angle' will over predict the mean of the spread angles. This is because we find the maximum contour out of all the images and then find a linear fit to the composite contour, instead of fitting a line and finding a spread angle for each image and then taking the average of those individual angles. When acoustics are present, this spreading angle encompasses a region where the inner jet traveled during all acoustic cycles captured in the number of images processed. Thus, for the cases where acoustics are on, this angle is referred to as the 'maximum acoustic spread angle'.

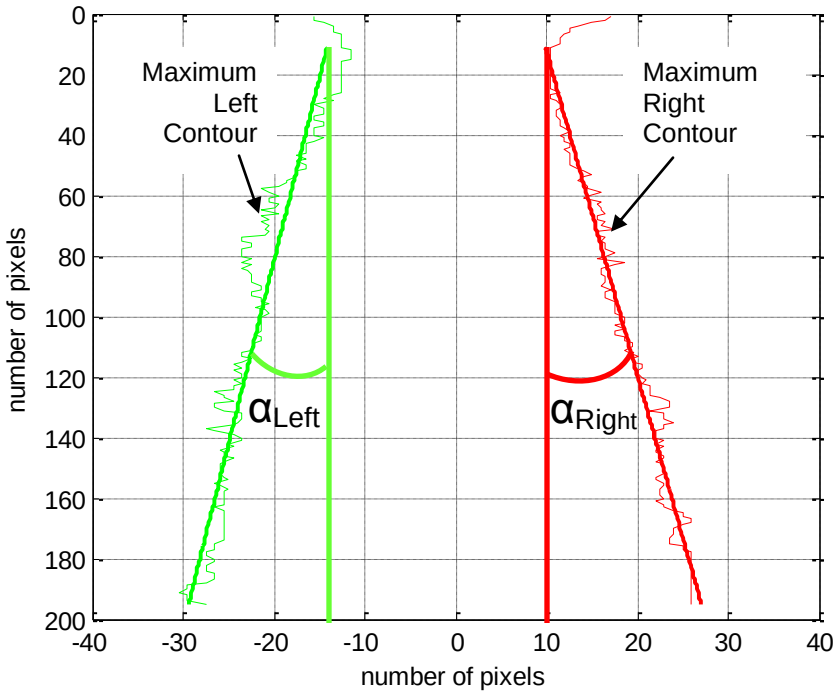

Figure 5. Left and right angles derived using the maximum displacement of the dark core at each row over a sample of 998 images.

The chamber pressure for the cases presented in this study is 3.6 MPa. For reference, the critical pressure, Pcr, of N2 is 3.39 MPa and its critical temperature, Tcr, is 126.2 K. At subcritical pressures, the inner jet reaches the saturation temperature while for these nearcritical pressures this temperature is kept as close as possible to the critical value.

Spreading Angle Analysis of Nearcritical Data

Eight nearcritical cases are reported in this study. The momentum flux ratio, J, was varied from 0.55 to 9.3. The coaxial jet was exposed to different acoustic conditions by varying the phase angle between the acoustic drivers. Different acoustic conditions at the location of the jet were obtained by varying the phase angle in steps of 45° starting at 0° and ending at 360°. A 'baseline' condition, which was a condition were both acoustic drivers were off was also part of each case. The maximum value of the peak-to-peak pressure perturbation normalized by the mean chamber pressure for each of the eight cases varied from 0.72%, for the case with J = 0.55, to 0.97%, for the case with J = 2.1. The maximum inner jet spreading angles, both baseline and acoustic, of all cases are shown in Fig. 6.

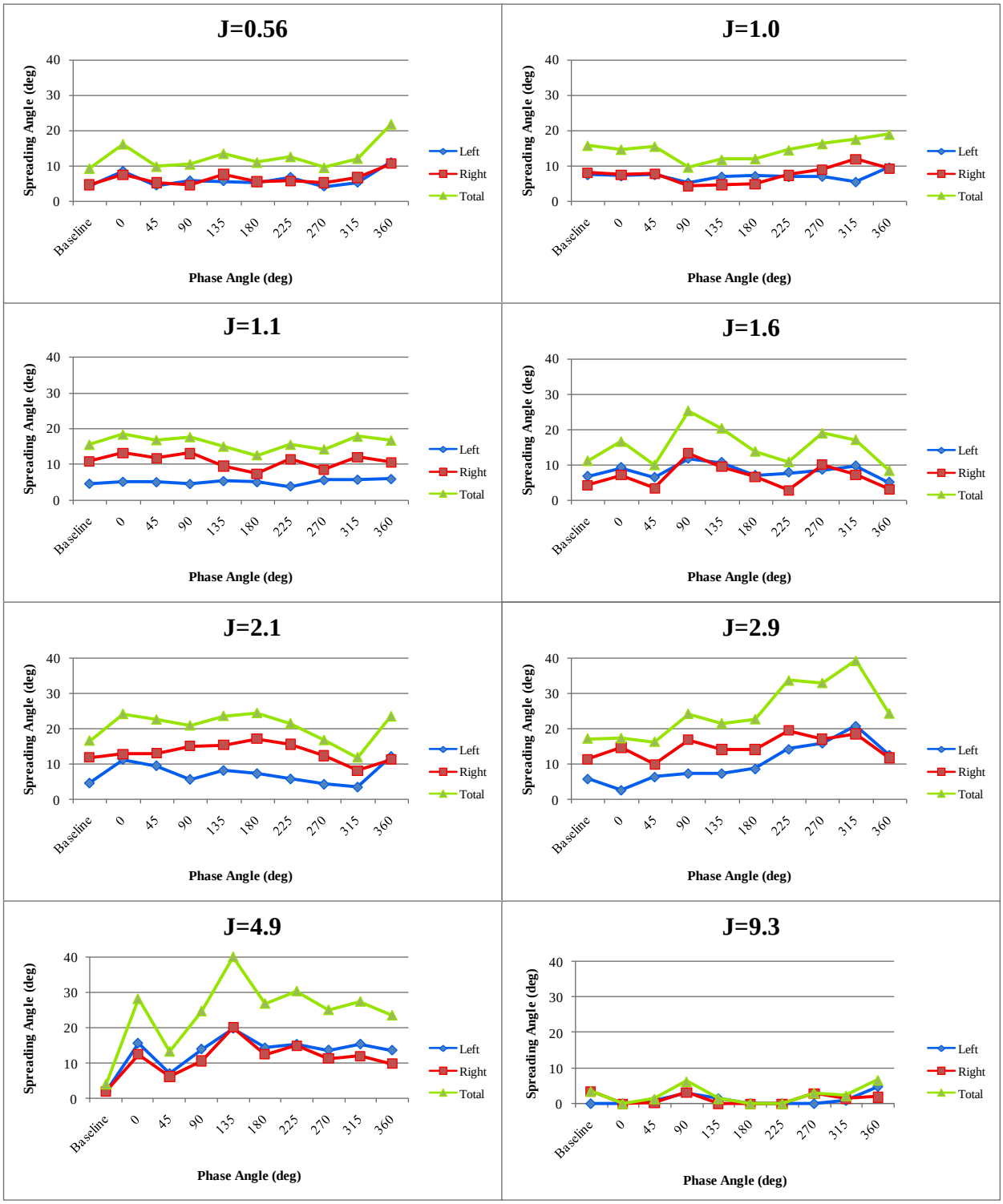

Figure 6. Maximum spread angles as a function of acoustic phase angle for different Js.

The behavior of the jet at J = 0.55 shows a very flat distribution of the spreading angles at different acoustic conditions. Most angles, including the condition with no acoustics present, show a value near 10°. The only exceptions are the spreading angles obtained at a phase angle of 0° and 360°. At these conditions, the dark core bends more than the rest of the cases and the inner jet flow penetrates the outer jet and seems to reach the inner chamber. The following two cases, J = 1.0 and 1.1, show a similar behavior. The values of the spreading angles fall between 10° and 20° and their corresponding baseline spreading angle values are 16°. For these cases where J is near or less than 1, acoustic forcing has little or no effect on the spreading angles. For J = 1.6 we observe that half of the acoustic conditions showing a clear difference between their corresponding spreading angle and the baseline. The spreading angle here shows a response to the acoustic forcing but there is still not a clear dependence on the phase angle between acoustic drivers. Similar behavior takes place when J = 2.1 with the average angle for the acoustic conditions over 20° in contrast with the baseline value of 17°. Both cases show maximum spreading angles around 25°.

At J = 2.9 and 4.9 a similar but more enhanced behavior is observed. Both have average values for the spreading angles under acoustic forcing that are significantly higher than their respective baselines. J = 2.9 has an average spreading angle with acoustics of 26° and a baseline of 17° and for J = 4.9 these values are 27° and 4° respectively. The effect of acoustics is the highest for these flow conditions. Finally, at J = 9.3, all the spreading are below 7° with an average of 2°. The reason for this behavior is the very short dark core length of the inner jet, which makes very difficult to capture any effect the acoustics might be having on it. The dark core itself is very straight until it mixes completely with its surroundings just a few inner jet diameters downstream the injector exit.

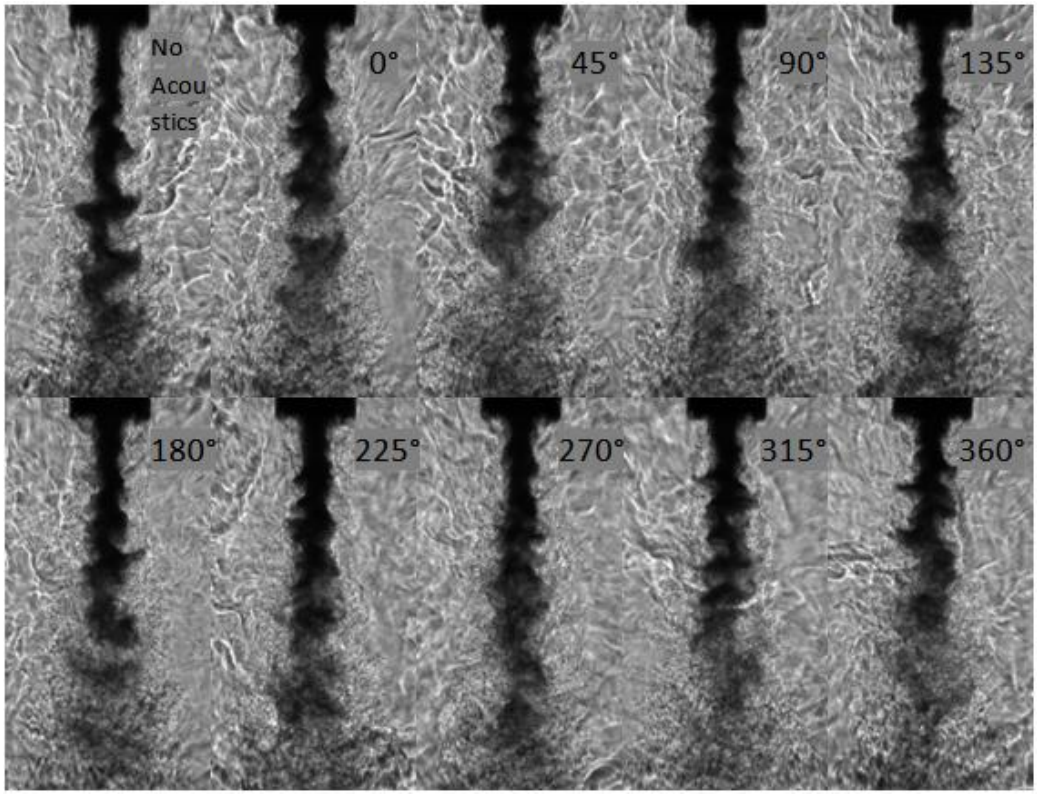

Figure 7. Collection of coaxial jet images at Pchamber = 3.58 MPa, J = 0.55.

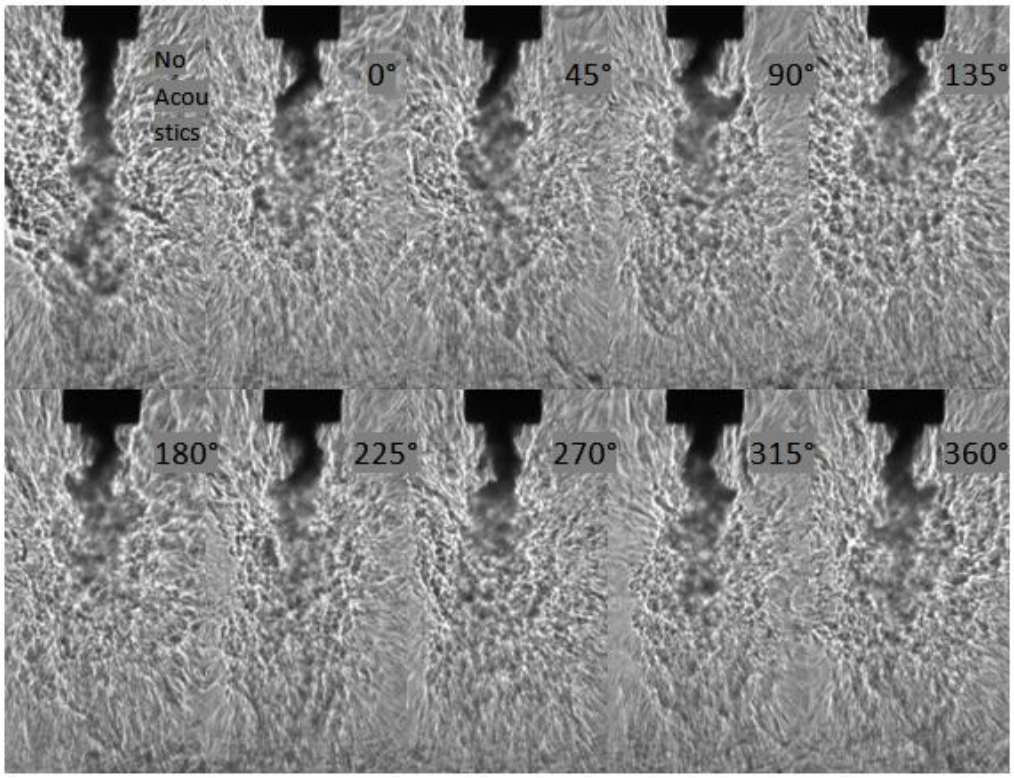

Figure 8. Collection of coaxial jet images at Pchamber = 3.56 MPa, J = 4.9.

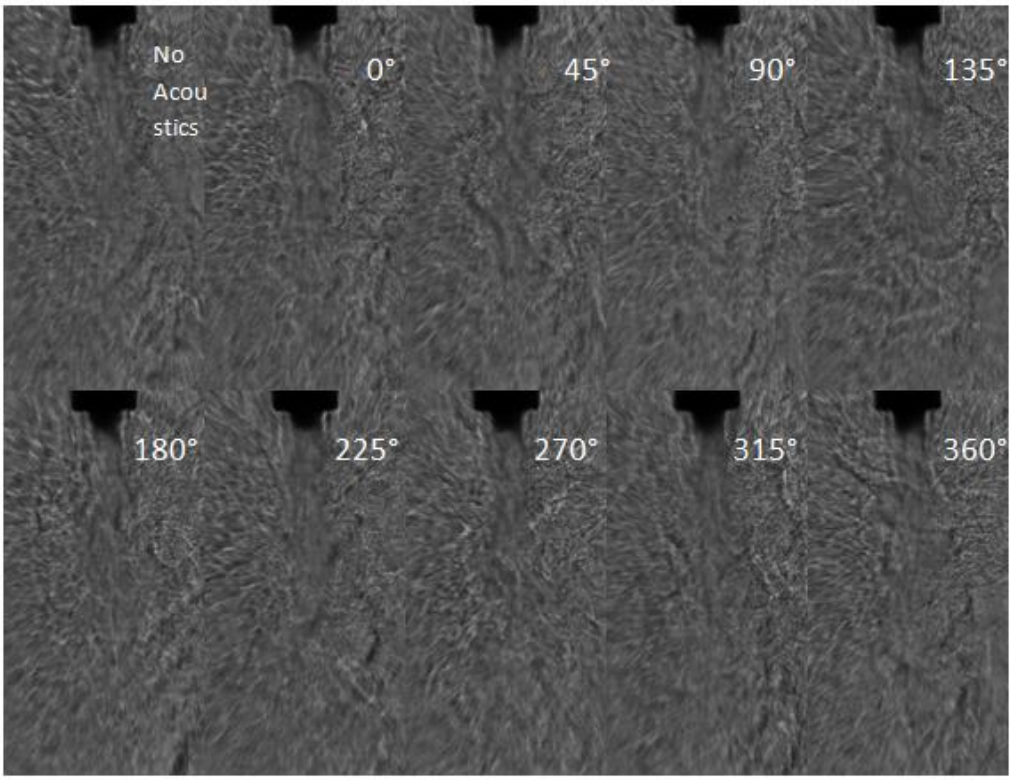

Figure 9. Collection of coaxial jet images at Pchamber = 3.56 MPa, J = 9.3.

IV. Conclusions

It was observed that at moderate J values ($1.5 < J < 5$) the acoustics have the strongest effect on the inner jet spreading angles. For the case where J is greater than 5, all spreading angles are well below 10° due to a very short and straight inner jet dark core length. At values of J below 1.5, the spreading angles were consistently higher than 10°; however, the average value of the spreading angle with acoustics was very similar to the spreading angle without acoustics. Therefore, the effects of the acoustics were not completely clear in this J range either. For the results presented in this study, the largest inner jet spreading angles with acoustics were obtained for J = 2.9 and 4.9 with 39° and 40° respectively. The largest spreading angles for the spreading angles without acoustics were obtained for J = 2.1 and 2.9 with both measuring 17°. The maximum peak to peak pressure perturbation as a percentage of the mean chamber pressure for all cases ranged from 0.72% to 0.97%.

The analysis of the nearcritical cases showed that acoustics has an increasingly larger effect on the inner jet spreading angles with increasing momentum flux ratio except for the highest value of J where the dark core length was very short and the spreading angle was very small and independent of the acoustic excitation. This overall trend was also observed on the subcritical pressure regime by our research group. In summary, the nearcritical data presented in this study further supports the finding that a range of moderate J values exists for which acoustic excitation effects are greatly enhanced and could potentially explain improved mixing and disruptive combustion instability effects observed at lower outer to inner jet velocity ratios.

V. References

1. Chehroudi, B., Talley, D., Coy, E., "Visual characteristics and initial growth rates of round cryogenic jets at subcritical and supercritical pressure", Physics of Fluids, Vol. 14, No. 2, February 2002, pp. 851-861.
2. Gutmark, E., Schadow, K. C., Wilson, K. J., "Mixing Enhancement in Coaxial Supersonic Jets*", AIAA-89-1812.*
3. Gautam, V., Gupta, A. K., "Simulation of Flow and Mixing from a Cryogenic Rocket Injector", *Journal of Propulsion and Power*, Vol. 23, No. 1, 2007, pp. 123-130.
4. Zong, N., Yang, V., "A Numerical Study of High-Pressure Oxygen/Methane Mixing and Combustion of a Shear Coaxial Injector", *AIAA-2005-0152*.
5. Richecoeur, F., Scouflaire, P., Ducruix, S., Candel, S., "High-Frequency Transverse Acoustic Coupling in a Multiple-Injector Cryogenic Combustor", *Journal of Propulsion and Power*, Vol. 22, No. 4, 2006, pp. 790-799.
6. Rodriguez, J. I., Graham, J. J., Leyva, I. A., Lyu, H.-Y., Talley, D., "On the Inner Jet Spread Angles of Coaxial Jets from Subcritical to Supercritical Conditions with Preliminary Numerical Results", *55th JANNAF Propulsion/4th Liquid Propulsion Subcommittee Meeting*, Orlando, FL, December 8-12, 2008.
7. Leyva, I. A., Chehroudi, B., Talley, D., "Dark-core analysis of Coaxial Injectors at Sub-, Near-, and Supercritical Conditions in a Transverse Acoustic Field", *54th JANNAF Meeting*, Denver, CO, May 14-18, 2007.
8. Leyva, I. A., Chehroudi, B., Talley, D., "Dark-core analysis of Coaxial Injectors at Sub-, Near-, and Supercritical Conditions in a Transverse Acoustic Field", *AIAA-2007-5456*.
9. REFPROP, Reference Fluid Thermodynamic and Transport Properties, Software Package, Ver. 7.0, NIST, U.S. Department of Commerce, Gaithersburg, MD, 2002.

VI. Appendix

A. Data Summary for Nearcritical Cases

	$T_{chamber}$ (K)	$\rho_{chamber}$ (kg/m^3)	$P_{chamber}$ (MPa)	T_{outer} (K)	$\dot{m}_{outer}$ (mg/s)	ρ_{outer} (kg/m^3)	u_{outer} (m/s)	T_{inner} (K)	$\dot{m}_{inner}$ (mg/s)	ρ_{inner} (kg/m^3)	u_{inner} (m/s)	Freq. (kHz)	VR
	Spreading Angles											P'_{RMS}	
	Baseline	φ=0°	φ=45°	φ=90°	φ=135°	φ=180°	φ=225°	φ=270°	φ=315°	φ=360°		(kPa)	J
NEAR													
near1	223	56.6	3.58	180	1060	75.4	5.38	123	290	520	2.8	3.08	2.0
Left	4.6	8.7	4.6	5.9	5.8	5.4	6.9	4.3	5.4	11.1			
Right	4.8	7.6	5.4	4.7	7.8	5.7	5.8	5.3	6.8	10.7		9.04	0.55
near2	207	62.0	3.57	152	1570	101	5.95	117	289	590	2.4	3.04	2.5
Left	7.6	7.3	7.6	5.3	7.1	7.2	7.1	7.1	5.6	9.7			
Right	8.2	7.5	8.0	4.3	4.8	4.8	7.4	9.2	12.0	9.3		10.8	1.0
near3	228	55.1	3.58	185	1590	72.4	8.40	126	293	440	3.3	3.00	2.6
Left	4.7	5.2	5.1	4.6	5.4	5.1	4.0	5.7	5.9	6.0			
Right	10.9	13.2	11.8	13.1	9.6	7.5	11.6	8.6	12.0	10.8		11.8	1.1
near4	223	56.1	3.55	184	2170	72.3	11.5	127	294	360	4.0	3.01	2.8
Left	6.9	9.4	6.5	11.9	10.8	7.1	8.0	8.7	9.8	5.2			
Right	4.4	7.3	3.6	13.4	9.6	6.8	3.0	10.3	7.3	3.3		11.4	1.6
near5	230	54.2	3.56	199	2120	65.1	12.5	126	292	440	3.3	3.03	3.8
Left	4.7	11.3	9.5	5.7	8.2	7.3	5.8	4.4	3.6	12.1			
Right	11.9	12.9	13.1	15.2	15.4	17.1	15.7	12.4	8.3	11.4		12.1	2.1
near6	229	54.5	3.56	183	2690	73.1	14.1	126	292	420	3.4	3.05	4.1
Left	5.8	2.6	6.3	7.3	7.3	8.6	14.2	15.9	20.8	12.6			
Right	11.4	14.7	10.0	16.9	14.2	14.1	19.5	17.1	18.5	11.8		11.1	2.9
near7	219	57.6	3.56	194	3080	67.4	17.5	125	289	480	3.0	3.06	5.9
Left	2.2	15.7	7.2	14.1	19.9	14.4	15.4	13.8	15.5	13.7			
Right	2.0	12.5	6.2	10.7	20.2	12.5	15.0	11.3	12.0	9.9		11.8	4.9
near8	213	59.6	3.56	192	6460	68.3	36.2	128	295	220	6.6	2.93	5.5
Left	3.5	0.0	0.3	3.1	0.0	0.0	0.0	3.0	1.4	1.9			
Right	3.5	0.0	1.4	6.2	1.4	0.0	0.0	3.0	2.3	6.7		9.73	9.3

Effect of Variable Phase Transverse Acoustic Fields on Coaxial Jet Forced Spread Angles

Juan I. Rodriguez*, Jeffrey J. Graham †, Ivett A. Leyva†, Douglas Talley†

*UCLA/Edwards AFRL, †Edwards AFRL,

AIAA 47th Aerospace Sciences Meeting & Exhibit

5 Jan 2009

Outline

- Motivation & Objectives
- Experimental Setup
- Results
- Concluding Remarks

Motivation & Objectives

Reduce **combustion instabilities**

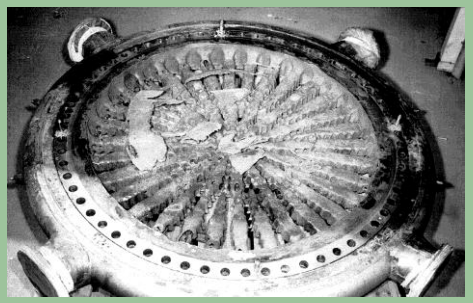

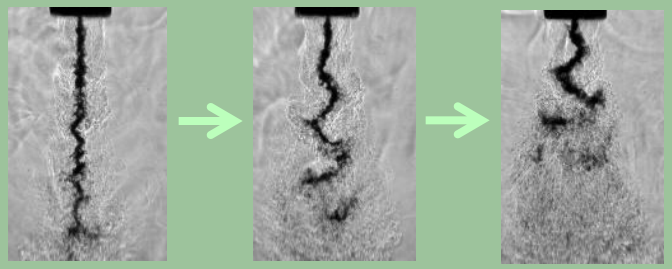

Characterize mixing enhancement

Unit Physics Problem:

Interaction of acoustics with coaxial jets spanning subcritical to supercritical pressures

Inner and Outer Jet Spread Angles

Observe effect on jet mixing

Experimental Setup – EC4

Phase Angle Setup

Outer Jet:

GN_2 or supercritical

Inner Jet:

GN_2 , LN_2, supercritical

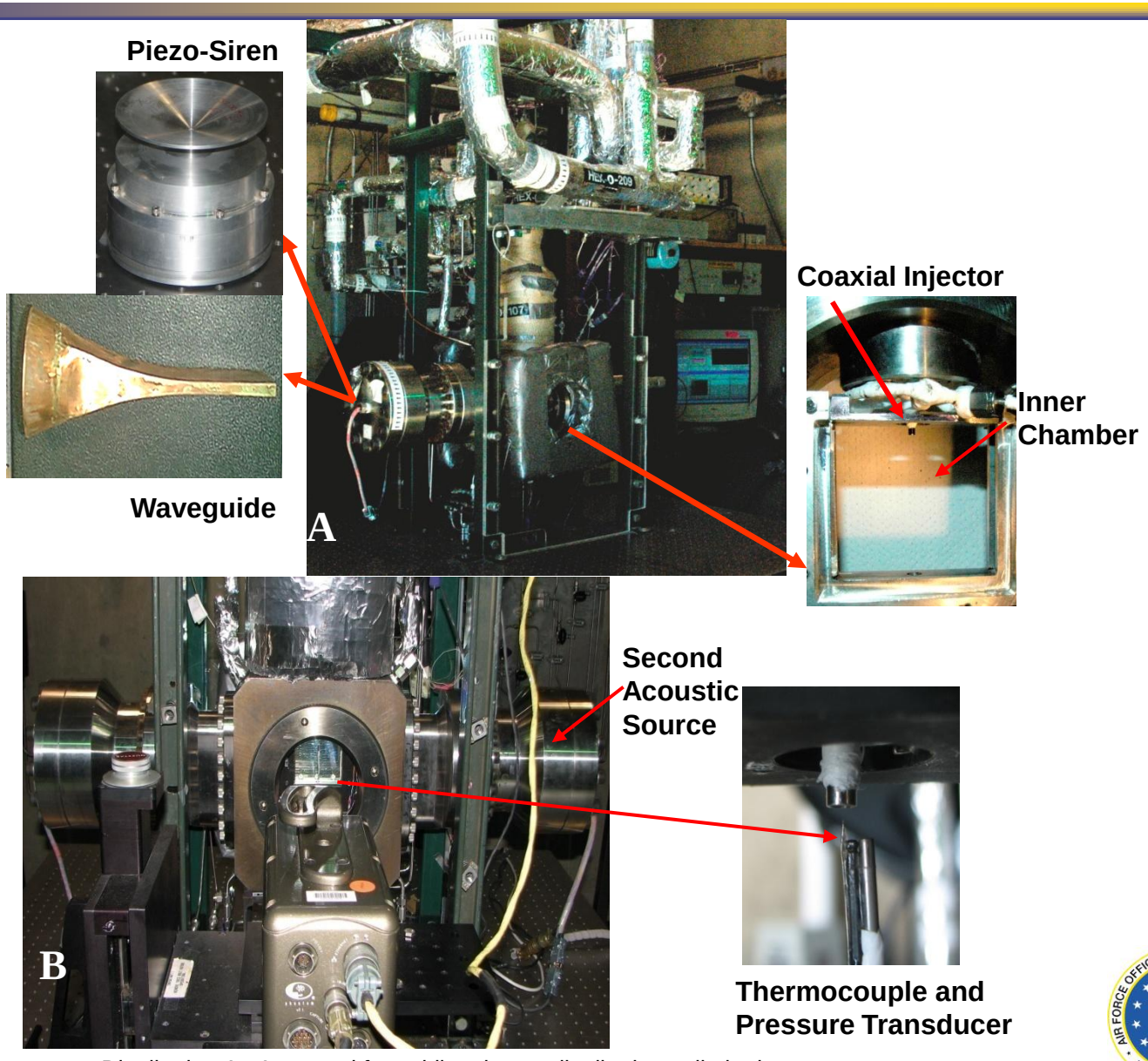

Coaxial injector

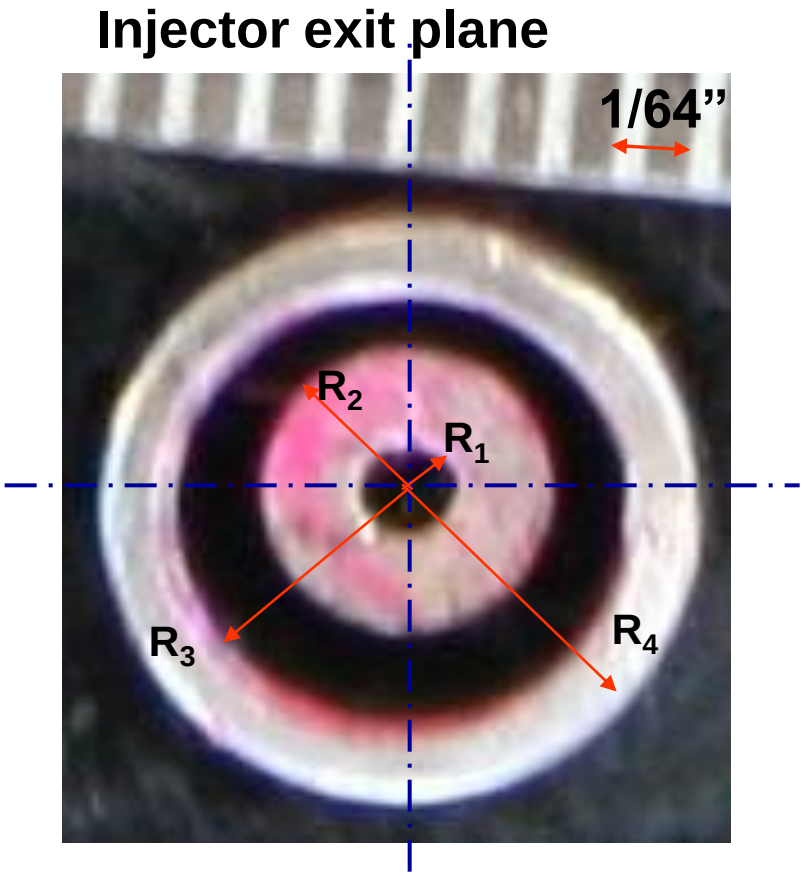

R_1 = 0.25 mm
R_2 = 0.80 mm
R_3 = 1.21 mm
R_4 = 1.59 mm

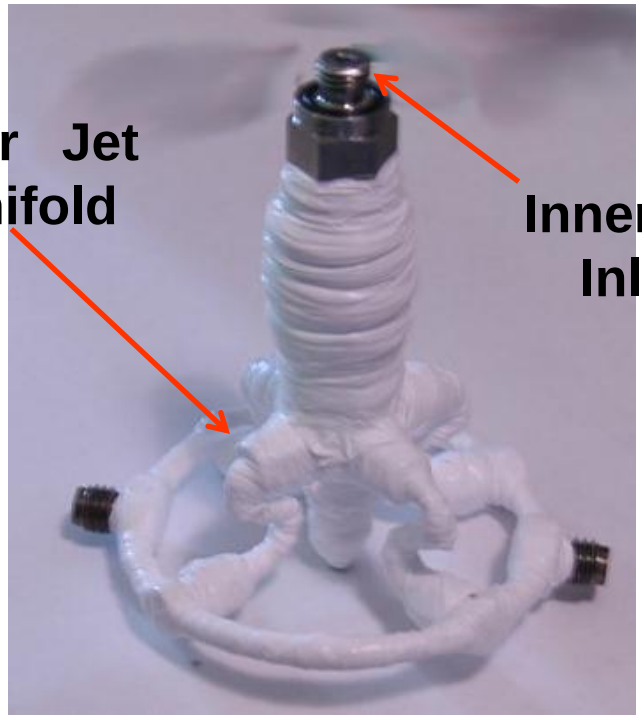

Injector

Inner Jet Spread Angle Study: Behavior of Acoustic Sources at 0° and 180°

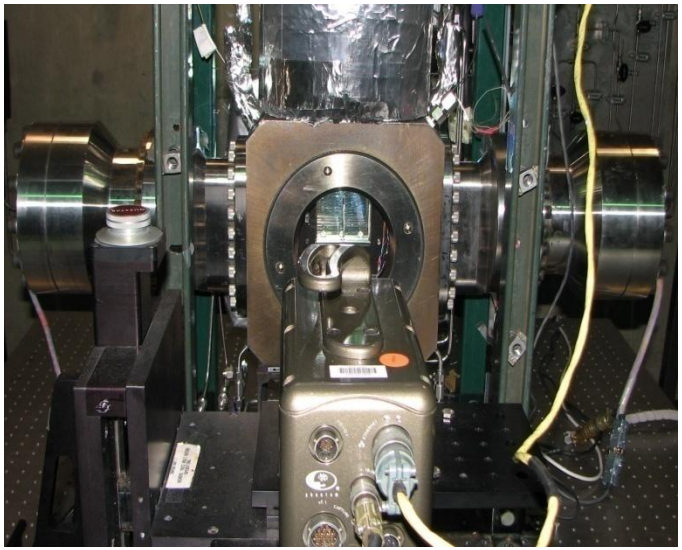

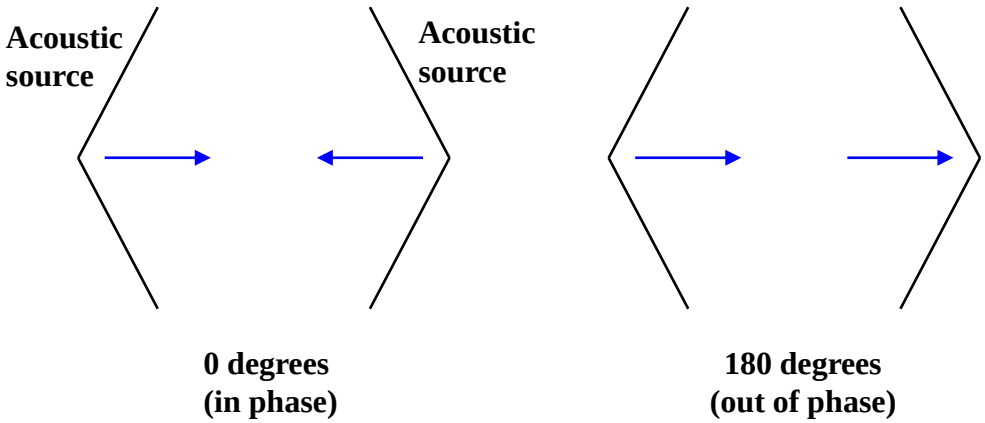

Test History

Configuration \ Forcing	No Acoustics	One Acoustic Source	Two Acoustic Sources
Injector for Present Study	Subcritical ☑	Subcritical ☑	Subcritical ☑
	Nearcritical ☑	Nearcritical ☑	Nearcritical ☑
	Supercritical ☑	Supercritical ☑	Supercritical ☑
New Injector	Subcritical ☑	Subcritical ☒	Subcritical ☑
	Nearcritical (IP*)	Nearcritical ☒	Nearcritical (IP*)
	Supercritical (IP*)	Supercritical ☒	Supercritical (IP*)

Inner Jet Spread Angle Results

***Currently In Progress**

Inner Jet Spread Angle Study: Test Cases

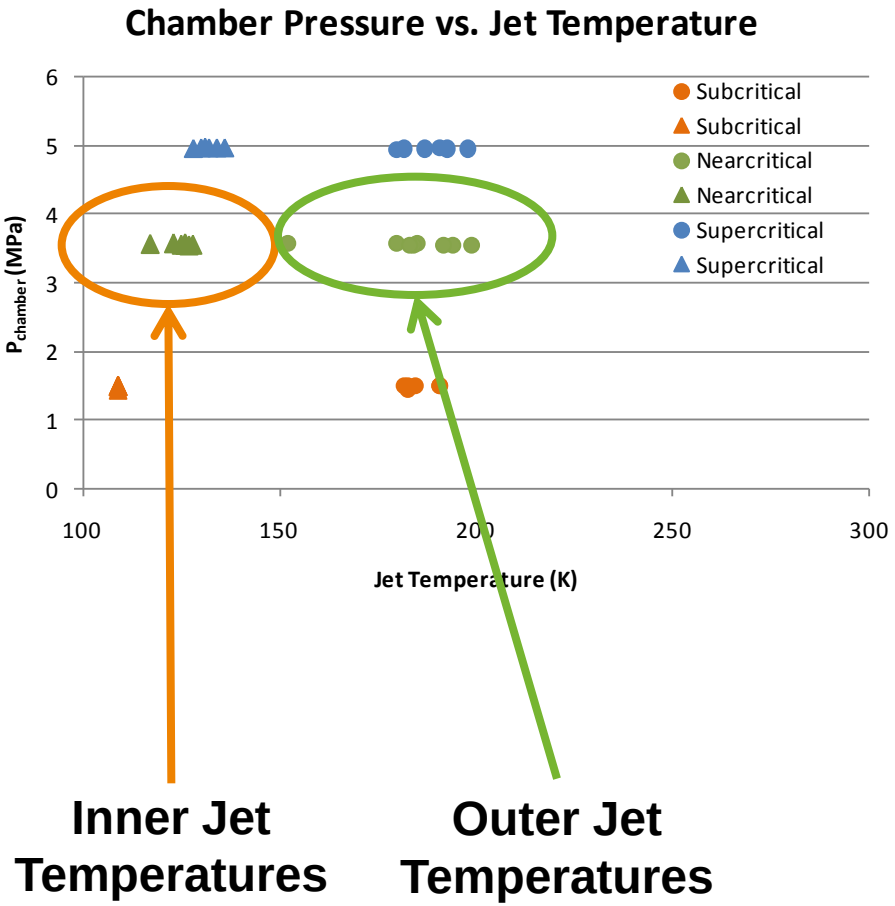

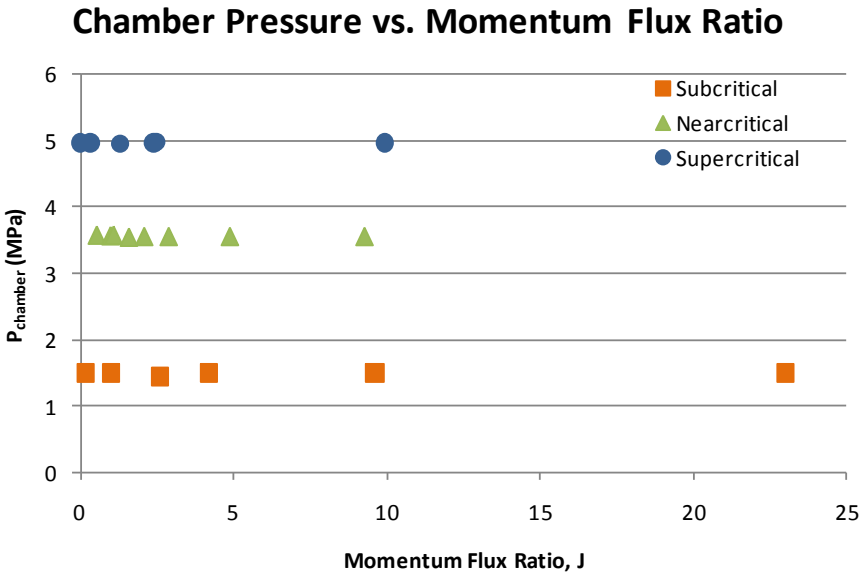

Inner Jet Spread Angle Study: Acoustic Characterization

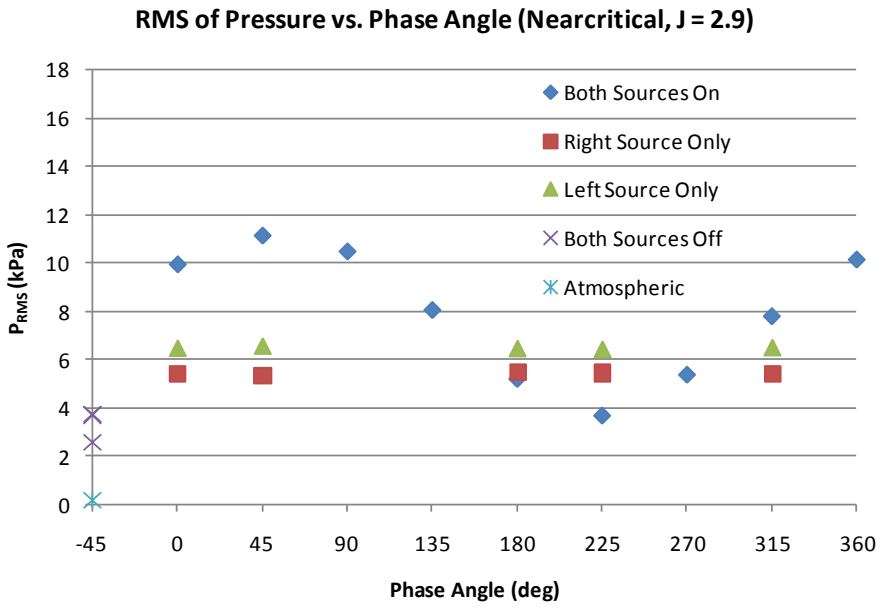

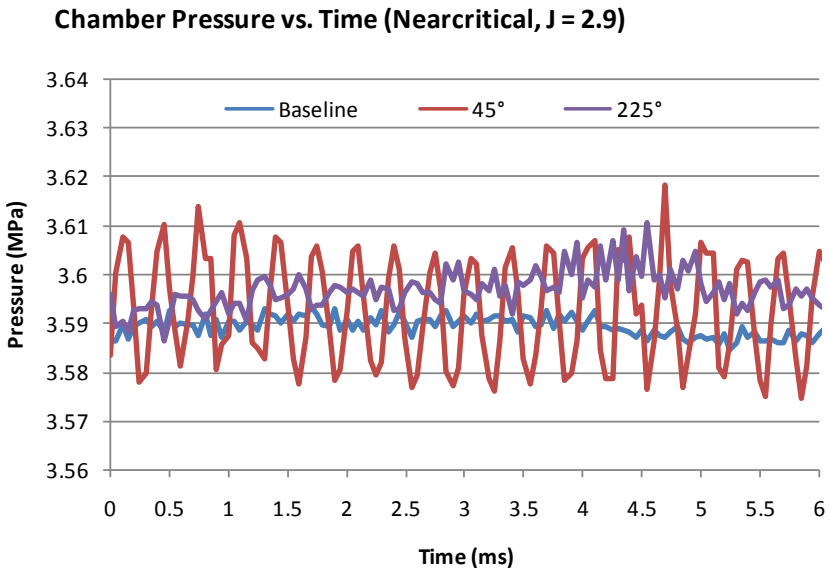

Minimum and maximum P'_{RMS} separated by 180°

Inner Jet Spread Angle Study: Acoustic Characterization Results

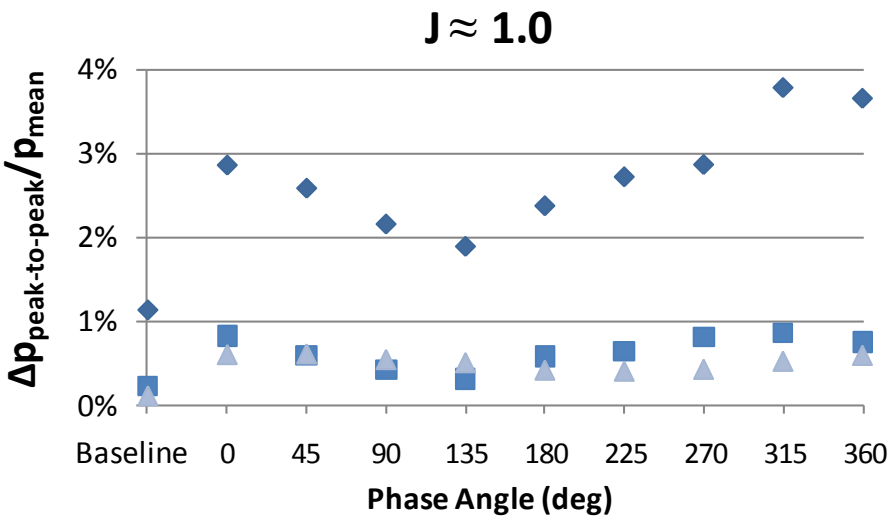

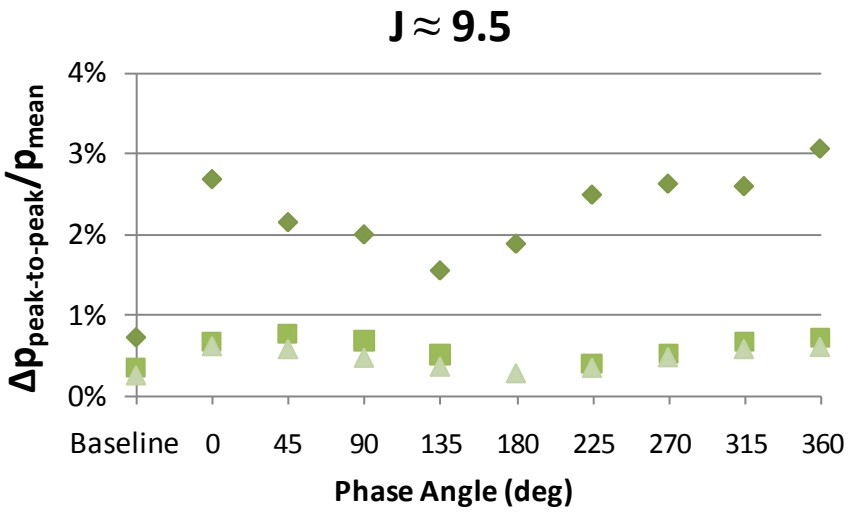

Pressure perturbation relative to overall pressure significantly higher for subcritical regime

Inner Jet Spread Angle Study: How are angles measured?

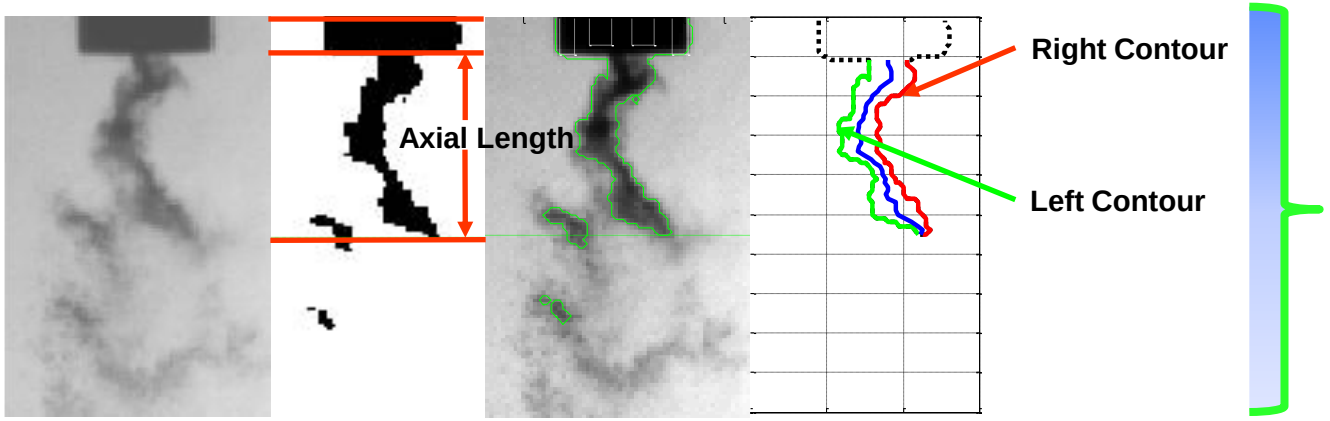

For each frame

After all frames have been processed

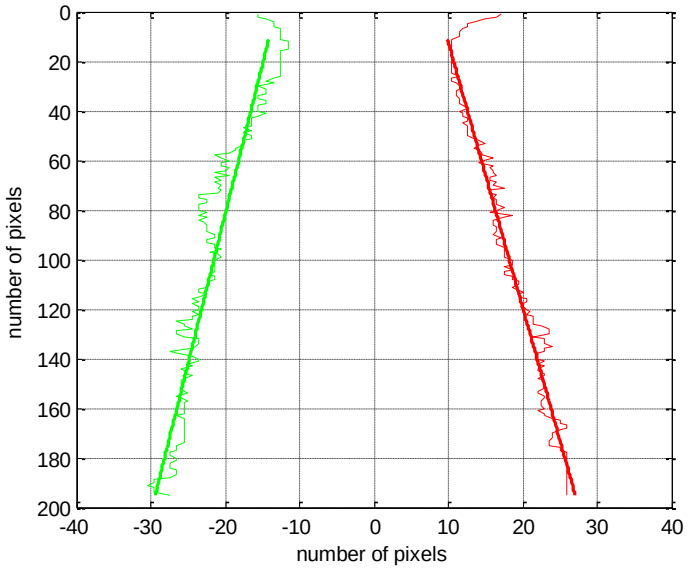

Nearcritical Case with J = 0.55 for different phase angles

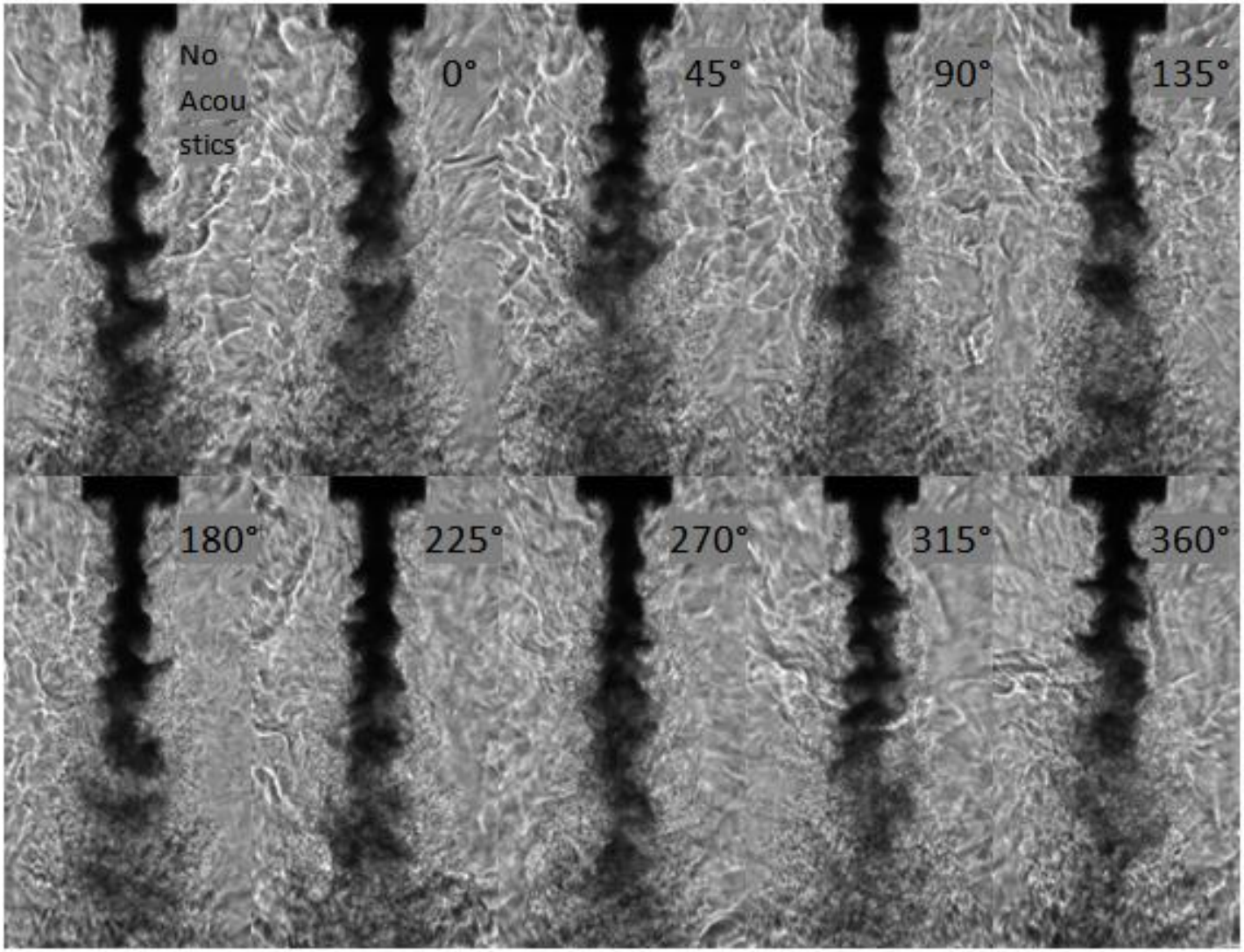

$P_{chamber}$=3.6 MPa, J=0.55, VR=2.0

Nearcritical Case with J = 4.9 for different phase angles

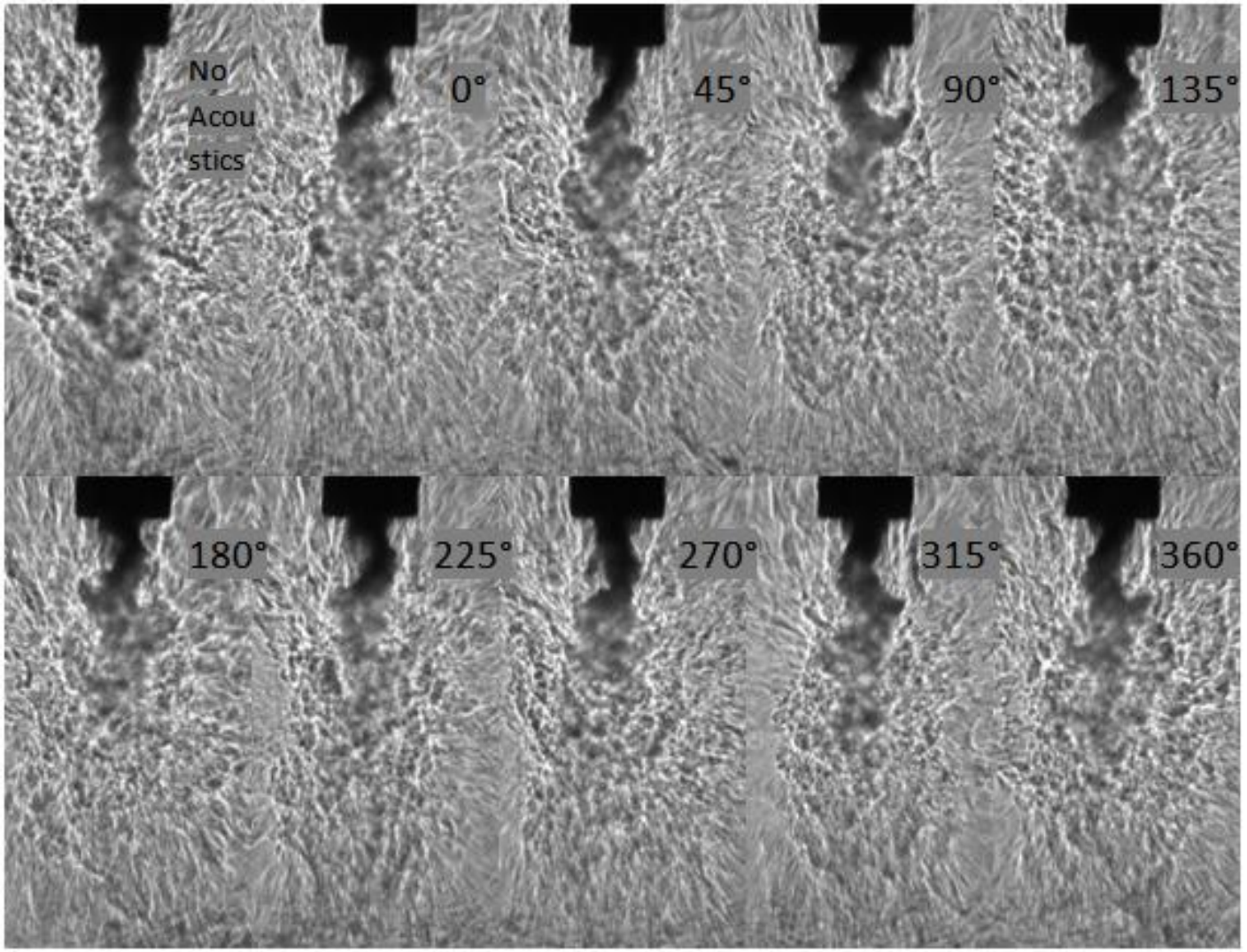

$P_{chamber}$ =3.6 MPa, J=4.9, VR=5.9

Nearcritical Case with J = 9.3 for different phase angles

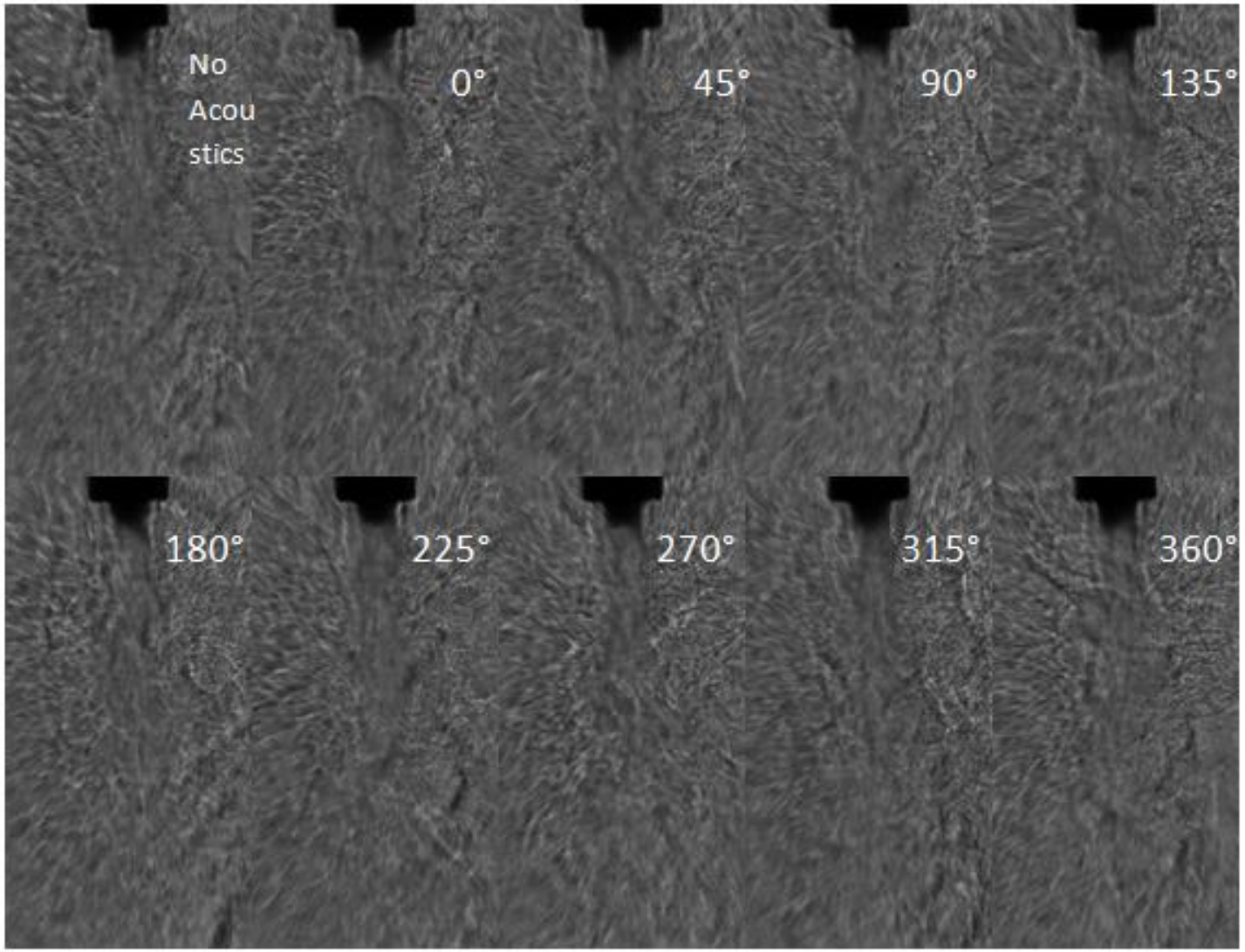

$P_{chamber}$ =3.6 MPa, J=9.3, VR=5.5

Inner Jet Spread Angle Study: Results at nearcritical pressures with acoustics

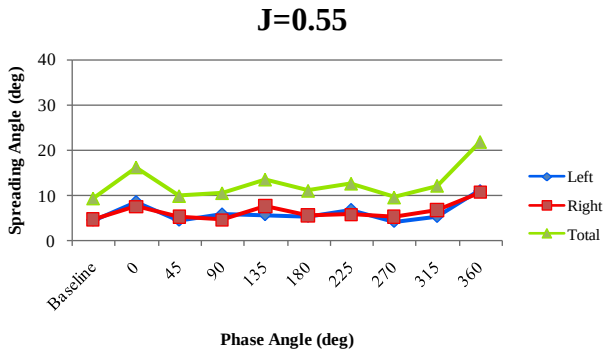

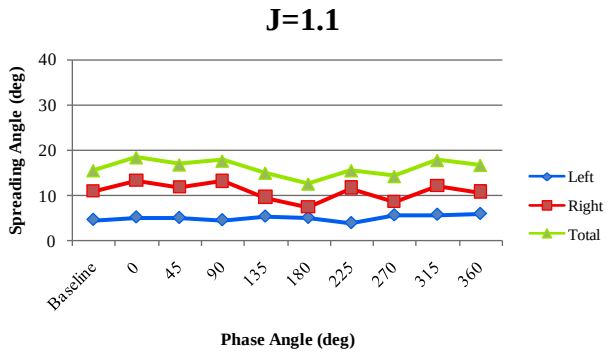

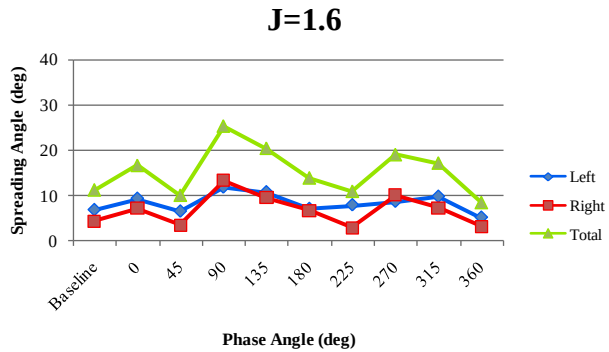

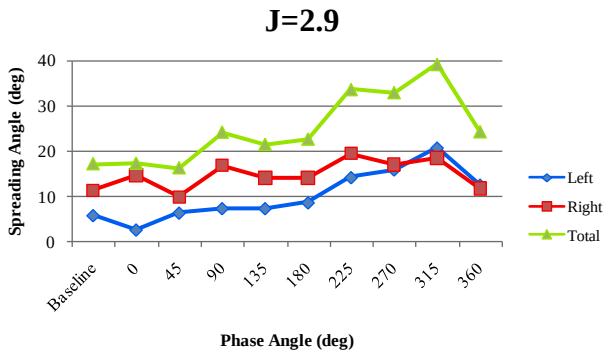

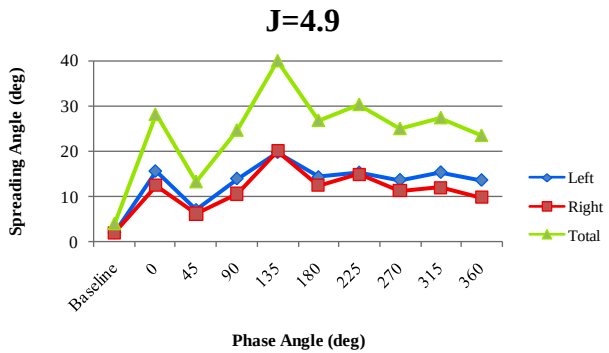

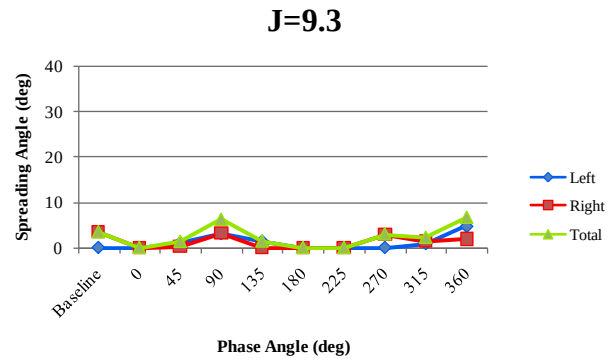

Effect of Phase for Different J and Chamber P

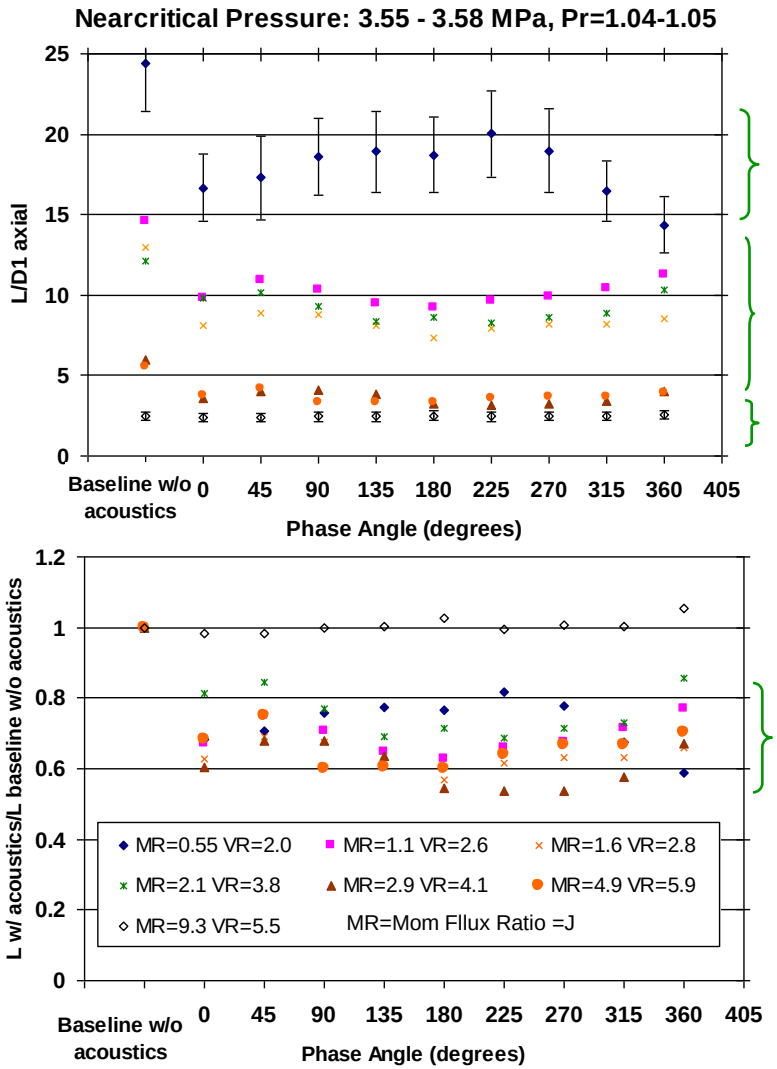

Approximates a single jet – different behavior

Most sensitive at middle J's –
J range depends on Pchamber

Insensitive at higher J's

Relative decrease on L is about 0.4 to 0.8 for most sensitive cases

Jet is most sensitive to acoustics at middle J's

Concluding Remarks

- **It was observed that at moderate J values (1.5 < J < 5) the acoustics have the strongest effect on the inner jet spreading angles.**
  - **For J > 5, all spreading angles are well below 10°.**
  - **For J < 1.5, the spreading angles were consistently higher than 10°; however, the average value of the spreading angle with acoustics was very similar to the spreading angle without acoustics.**

- **Largest inner jet spreading angles**
  - **with acoustics: J = 2.9 and 4.9 with 39° and 40° respectively.**
  - **without acoustics: J = 2.1 and 2.9 both measuring 17°.**

- **Maximum $\Delta p_{peak\text{-}to\text{-}peak}/p_{chamber}$ for all cases ranged from 0.72% to 0.97%.**

- **Nearcritical data supports the ongoing observation that a range of moderate J values exists for which acoustic excitation effects are greatly enhanced and could potentially explain:**
  - **improved mixing and,**
  - **disruptive combustion instability effects observed at lower outer to inner jet velocity ratios**

Research Team

- **Researchers**
  - **Dr. Ivett A. Leyva, Lead, Combustion Devices Group.**
  - **Dr. Douglas Talley, Senior Research Scientist.**
  - **Dr. Bruce Chehroudi, Principal Scientist, ERC Inc. (On Leave)**
  - **Lt. Jeffrey Graham, Combustion Research Scientist.**
  - **Juan Rodriguez, UCLA Ph.D. Student.**
- **Mechanical Crew**
  - **Randy Harvey, Earl Thomas, Todd Newkirk (Jacobs Engineering), Dave Hill, ERC**
- **This work is sponsored by the Air Force Office of Scientific Research under Dr. Mitat Birkan, program manager.**

Back Up Slides

Dark-Core Length vs. Momentum Flux Ratio with One Acoustic Source on/off for 2 Length Definitions

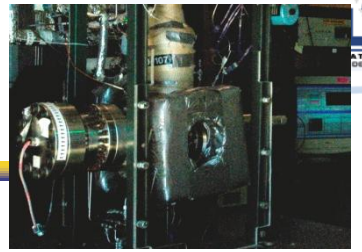

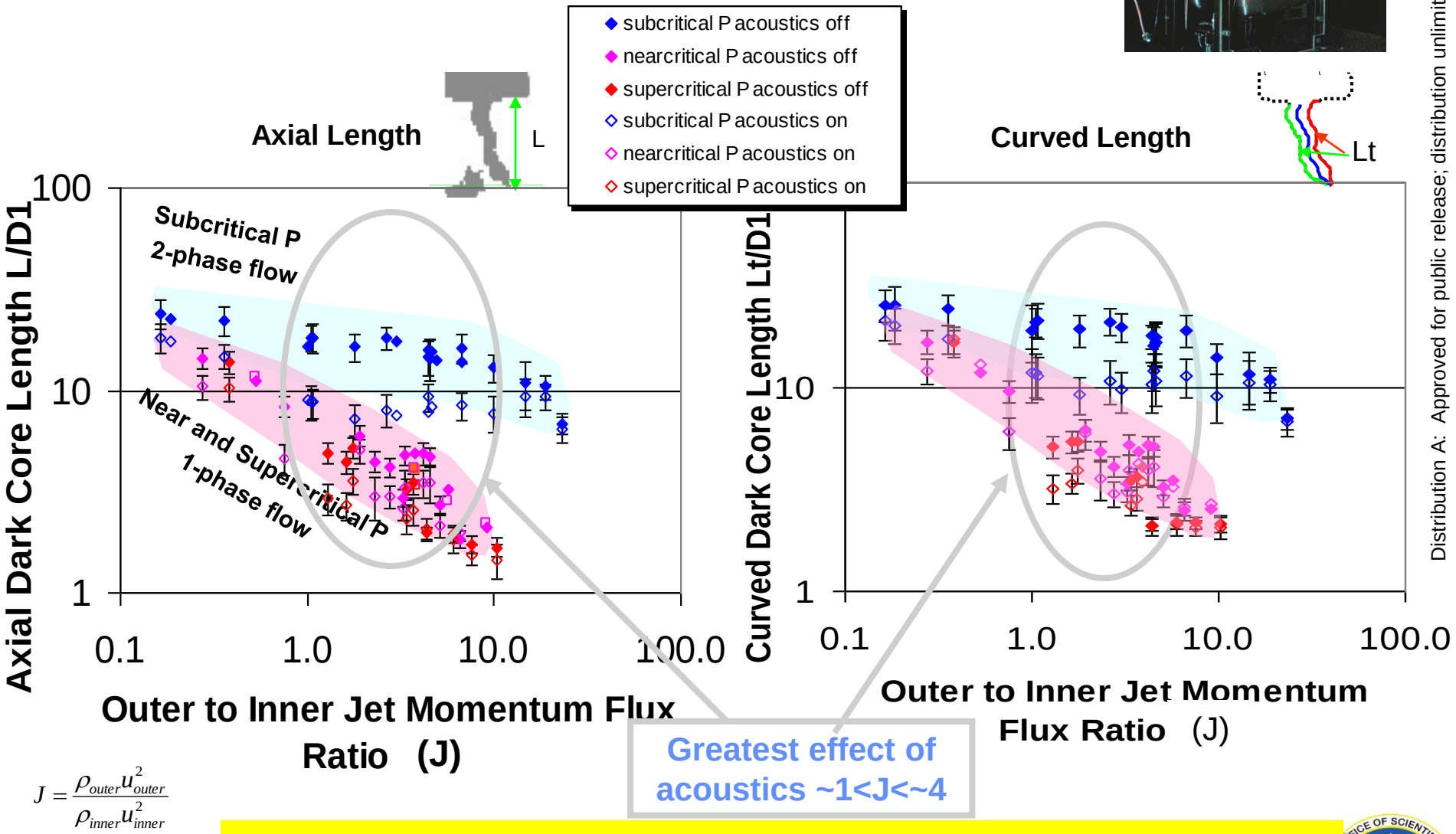

$$J = \frac{\rho_{outer} u_{outer}^2}{\rho_{inner} u_{inner}^2}$$

Greatest effect of acoustics ~1<J<~4

Acoustics shorten the curved and axial dark core lengths irrespective of definition used

ERC INCORPORATED

Phase Diagram of Nitrogen

- **Supercritical Conditions**
  - Very large Cp at Critical Point (CP)
  - Surface tension vanishes
  - Heat of vaporization vanishes above CP
  - Distinction between liquid and gas phases disappears above CP
  - For mixtures: Critical mixing T & P (critical lines for 2 components)
  - P_{cr} = 3.39 MPa
  - T_{cr} = 126.2 K

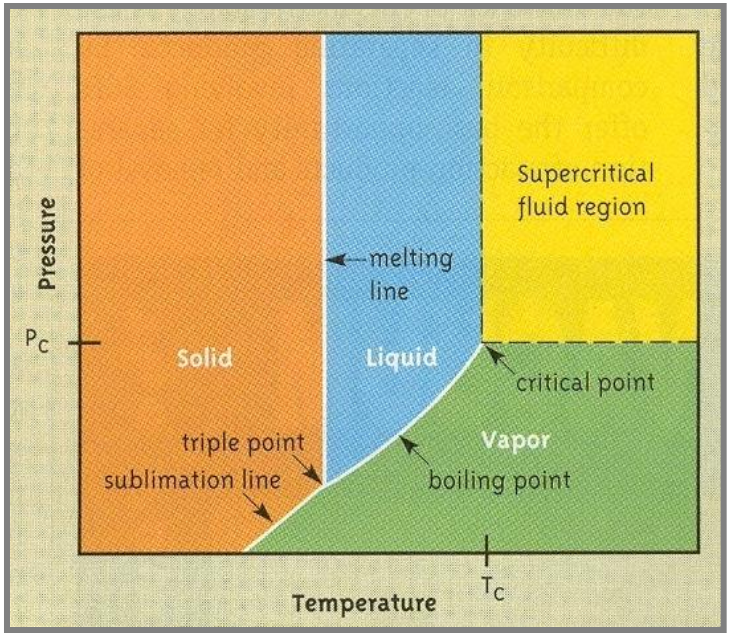

Detailed Injector Diagram

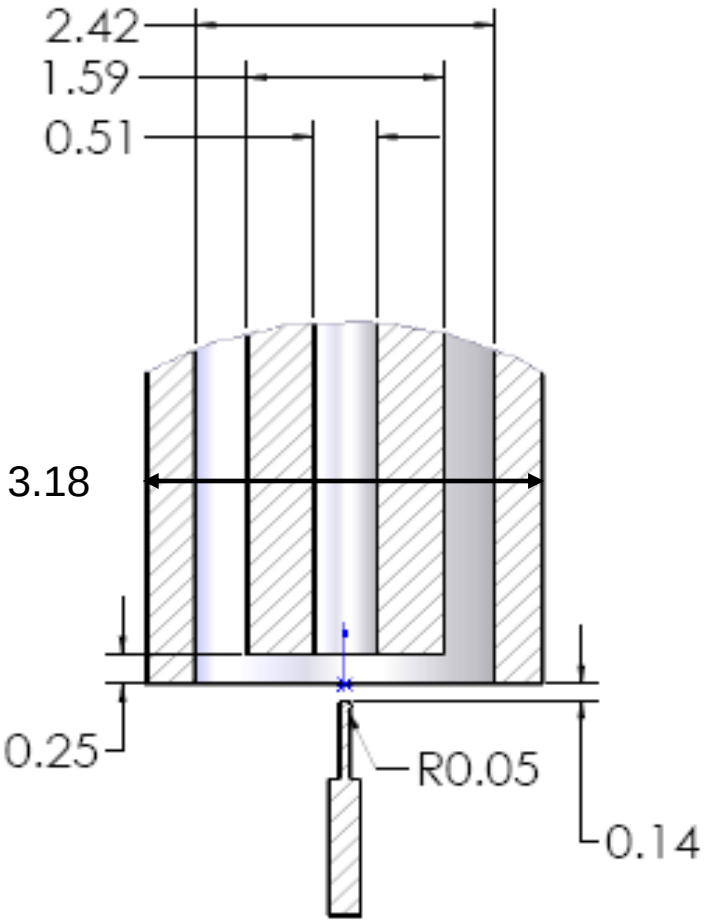

Units are in millimeters (mm)

Threshold Technique

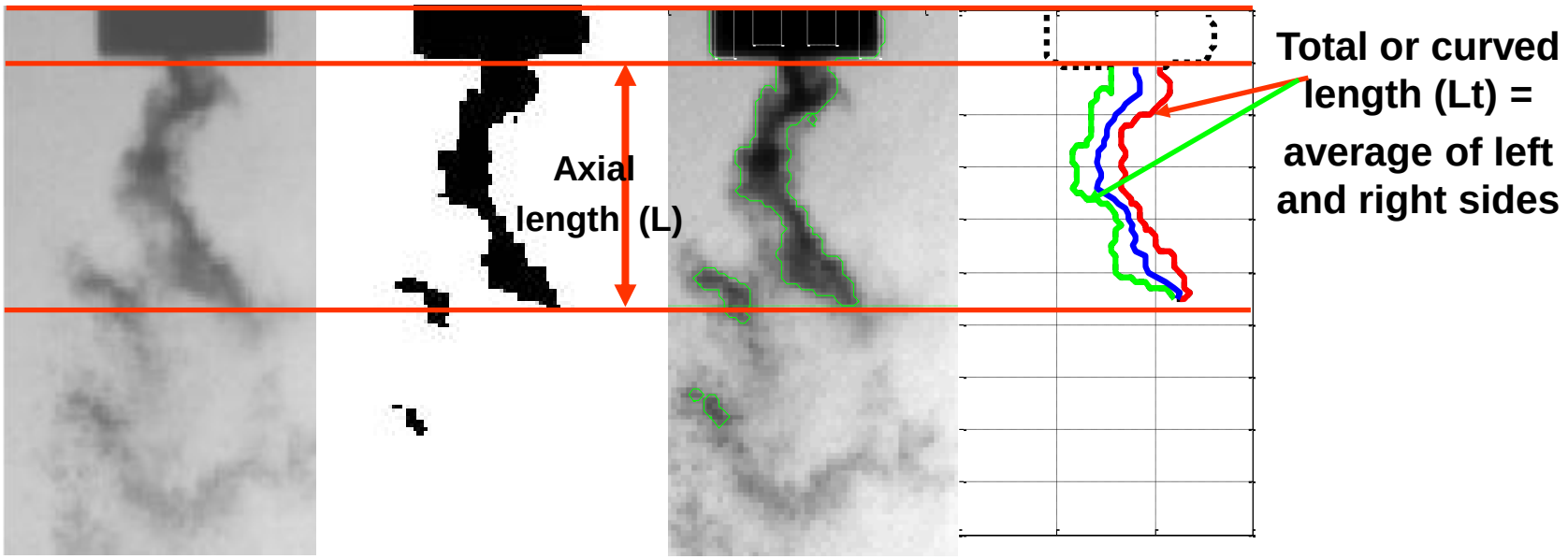

$P_{chamber}$ = 1.50 MPa; VR = 7.5; MR = 2.6; Acoustics On

- **Threshold Images based on Otsu's method** (N. Otsu, "A Threshold Selection Method from Gray-Level Histograms," IEEE Transactions on Systems, Man, and Cybernetics, vol. 9, no. 1, pp. 62-66, 1979.)
- **Accounts for variability from image to image (including D1, the parameter by which the jet is normalized)**

Test Conditions

	$T_{chamber}$ (K)	$\rho_{chamber}$ (kg/m^3)	$P_{chamber}$ (MPa)	T_{outer} (K)	$\dot{m}_{outer}$ (mg/s)	ρ_{outer} (kg/m^3)	u_{outer} (m/s)	T_{inner} (K)	$\dot{m}_{inner}$ (mg/s)	ρ_{inner} (kg/m^3)	u_{inner} (m/s)	Freq. (kHz)	VR
	Spreading Angles											P'_{RMS} (kPa)	J
	Baseline	φ=0°	φ=45°	φ=90°	φ=135°	φ=180°	φ=225°	φ=270°	φ=315°	φ=360°			
NEAR													
near1	223	56.6	3.58	180	1060	75.4	5.38	123	290	520	2.8	3.08	2.0
Left	4.6	8.7	4.6	5.9	5.8	5.4	6.9	4.3	5.4	11.1			
Right	4.8	7.6	5.4	4.7	7.8	5.7	5.8	5.3	6.8	10.7		9.04	0.55
near2	207	62.0	3.57	152	1570	101	5.95	117	289	590	2.4	3.04	2.5
Left	7.6	7.3	7.6	5.3	7.1	7.2	7.1	7.1	5.6	9.7			
Right	8.2	7.5	8.0	4.3	4.8	4.8	7.4	9.2	12.0	9.3		10.8	1.0
near3	228	55.1	3.58	185	1590	72.4	8.40	126	293	440	3.3	3.00	2.6
Left	4.7	5.2	5.1	4.6	5.4	5.1	4.0	5.7	5.9	6.0			
Right	10.9	13.2	11.8	13.1	9.6	7.5	11.6	8.6	12.0	10.8		11.8	1.1
near4	223	56.1	3.55	184	2170	72.3	11.5	127	294	360	4.0	3.01	2.8
Left	6.9	9.4	6.5	11.9	10.8	7.1	8.0	8.7	9.8	5.2			
Right	4.4	7.3	3.6	13.4	9.6	6.8	3.0	10.3	7.3	3.3		11.4	1.6
near5	230	54.2	3.56	199	2120	65.1	12.5	126	292	440	3.3	3.03	3.8
Left	4.7	11.3	9.5	5.7	8.2	7.3	5.8	4.4	3.6	12.1			
Right	11.9	12.9	13.1	15.2	15.4	17.1	15.7	12.4	8.3	11.4		12.1	2.1
near6	229	54.5	3.56	183	2690	73.1	14.1	126	292	420	3.4	3.05	4.1
Left	5.8	2.6	6.3	7.3	7.3	8.6	14.2	15.9	20.8	12.6			
Right	11.4	14.7	10.0	16.9	14.2	14.1	19.5	17.1	18.5	11.8		11.1	2.9
near7	219	57.6	3.56	194	3080	67.4	17.5	125	289	480	3.0	3.06	5.9
Left	2.2	15.7	7.2	14.1	19.9	14.4	15.4	13.8	15.5	13.7			
Right	2.0	12.5	6.2	10.7	20.2	12.5	15.0	11.3	12.0	9.9		11.8	4.9
near8	213	59.6	3.56	192	6460	68.3	36.2	128	295	220	6.6	2.93	5.5
Left	3.5	0.0	0.3	3.1	0.0	0.0	0.0	3.0	1.4	1.9			
Right	3.5	0.0	1.4	6.2	1.4	0.0	0.0	3.0	2.3	6.7		9.73	9.3